Kinematic and Dynamic Analyses of Tripteron, an Over-Constrained 3-DOF Translational Parallel Manipulator, through Newton-Euler Approach

A. Arian, B. Danaei, M. Tale-Masouleh*

Human and Robot Interaction Laboratory, Faculty of New Sciences and Technologies, University of Tehran, Tehran, Iran

ABSTRACT: In this research, as the main contribution, a comprehensive study is carried out on the mathematical modeling and analysis of the inverse kinematics and dynamics of an over-constrained three translational degree-of-freedom parallel manipulator. Due to inconsistency between the number of equations and the unknowns, the problem of obtaining the constraint forces and torques of over-constraint manipulators does not admit solution, which can be regarded as one of the drawbacks of such mechanisms. In this paper, in order to overcome this problem and circumvent inconsistency between the number of equations and the unknowns, two of the revolute joints attached to the end-effector are changed into a universal and a spherical joint without changing the motion pattern of the manipulator under study. Then, the dynamical equations of the manipulator are obtained based on the Newton–Euler approach, and a simple and a compact formulations are provided. Then, all the joint forces and torques are presented. In order to evaluate accuracy of the obtained formulated model, a motion for the end-effector as a case study is performed, and it has been shown that the results of the analytical model are in a good agreement with those obtained from SimMechanics model. Finally, the Root Mean Square error is calculated between the analytical model and the results obtained from the simulation and experimental study

1- Introduction

In theory, a Parallel Manipulator (PM) generally allows for a better dynamic performance than a serial manipulator [1]. Furthermore, PMs offer higher accuracy, speed, acceleration, and stiffness. However, PMs commonly suffer from a limited workspace compared to their serial counterparts [2].

Over the past decades, many novel designs have been proposed to overcome workspace limitations of the PMs, including: axis-symmetric PMs [3-5] which employ 2-7 actuated arms rotating around a common axis of rotation and robots with actuated carts on parallel guide-ways, e.g. Tripteron, Quadrepteron and Pentaptereon from the Université Laval Canada [6, 7]. Despite all disadvantages that limit the use of PMs, such as smaller workspace, they offer some advantages over serial manipulators like high rigidity, high speed, acceleration and accuracy [2]. Nowadays, PMs due to their high positional accuracy and high speed are used in several industries, such as CNS machining tools which are referred to as Parallel Kinematic Machine [8]. In theory, a PM allows for a better dynamic performance than a serial one [1].

The 3-DOF translational PM under study, called Tripteron, was first built at the Laval University [9]. It belongs to a class of PMs known as Multipteron [10] which is arisen from the type synthesis performed for PM exhibiting three translational motion patterns. The kinematic analysis of the Multipteron family was discussed in [10] and the inverse and forward kinematic of Tripteron and its singularity analysis were investigated in [11]. In [12], experimental results of the controlling of a 3-DOF DPM via an HRI interface was given. The objective of the inverse dynamics' model of a mechanism is to calculate the required actuation force/torque in order for achieving a specified trajectory, typically, as a function of the position, velocity, and acceleration of the joint variables and the coordinates of the end-effector of the manipulator. Dynamics' model is essential for simulation, control and optimal design of the manipulators. However, dynamics' formulation of PMs is often complicated due to their multiple closed-loop chains [2]. There are several approaches to formulate the dynamical equations of PMs. Euler-Lagrange [13, 14], virtual work [15-17] and Newton-Euler methods [18-20] are among the three popular methods for dynamical analysis of PMs. The Newton-Euler method has been shown to be effective for performing the inverse dynamics of PMs and unlike Lagrangian formulation, it does not requires evaluation of derivatives of any function. Virtual work and Euler-Lagrange methods only depict relationship between external wrenches and actuation forces without providing reaction parameters in the joints. Thus, these methods are advantageous over the Newton-Euler method when internal forces are not required. However, Newton-Euler method obtains all the internal wrenches which are important and indispensable for optimal design and understanding the behavior of dynamical reaction of the manipulator. Several studies have been conducted on the dynamical analysis of PMs. In [21], the inverse dynamics of PMs, including redundant PMs is presented. In [22, 23], the Newton-Euler method is used for modeling the Gough-Stewart platform. In [24], an approach based on the manipulator's generalized momentum was studied and, then, applied to this manipulator. In [25], Newton method is employed to develop the dynamical model of the metamorphic parallel mechanism [26]. Dynamical analysis of over-constraint manipulators is

challenging due to redundant constraints imposed by each limb of the manipulator and has inspired several studies [25, 27, 28]. From a mechanical standpoint, over-constraint mechanisms are defined as systems which have more DOF of mobility than they expected to have from Chebychev–Grübler–Kutzbach (CGK) criterion, a criterion which cannot take into account redundant constraints in its formulation. When the equilibrium equations are written for an over-constraint manipulator, the number of equations will be less than the number of the unknowns, mathematically speaking, an underdetermined system of equations, and, consequently, the dynamical equations of the manipulators will be unsolvable.

The main contribution of this paper is the developing of an explicit compact formulation for the dynamical model of an over-constraint 3-DOF translational PM via Newton-Euler approach by changing the kinematic structure of the manipulator to an equivalent constrained manipulator without changing the motion pattern of the system. In addition, the forces and torques in all passive joints are obtained, and this can be regarded as the advantage of the Newton-Euler formulation over other methods mentioned above.

The remainder of this paper is organized as follows. In section 2, a description of the manipulator is presented. Section 3 provides the vector representation of the inverse kinematic problem of the 3-DOF translational PM considering the position, velocity, and acceleration of the end-effector. In section 4, the inverse dynamics' equations of the manipulator are formulated based on the Newton-Euler approach and a closed form for its dynamics is presented. Section 5 presents the simulation performed on SimMechanics in order to evaluate accuracy of the presented model. Furthermore, the results obtained from the analytical model are put into contrast by those obtained from SimMechanics model and experimental results. Finally, the paper concludes with some discussions and hints for ongoing works.

2- 3-DOF Translational Parallel Manipulator

Fig. 1. The 3-DOF decoupled PM constructed in the Human and Robot Interaction Laboratory, University of Tehran.

As illustrated in Fig. 1, the 3-DOF translational PM called Tripteron is composed of three identical kinematic chains as PRRR which can move independently. The notation

PRRR describes the joints in the kinematic chains from the actuator to the end-effector in which P and R stand for prismatic and revolute joints, respectively. Moreover, the actuated joint, which is the prismatic joint, in this case, is underlined. From the types synthesis performed on this PM, the direction of the axes of the revolute joints in each chain is parallel to the direction of its corresponding prismatic joint. In order to preserve the orthogonality of the mechanisms, all the directions of prismatic actuators form an orthogonal coordinate frame.

The present manipulator is an isotropic and fully decoupled manipulator. Thus, each of the linear actuators controls one of the translational DOFs. The latter issue leads to a fully decoupled motion which results in an identical motion for its inverse Jacobian matrix. Consequently, as revealed in reference [11], it can be inferred that the manipulator has a singularity-free workspace which is a definite asset in control and practice.

Furthermore, Tripteron is an over-constrained manipulator. By using the Chebychev–Grübler–Kutzbach formula [29] for the mobility of this mechanism, we obtain:
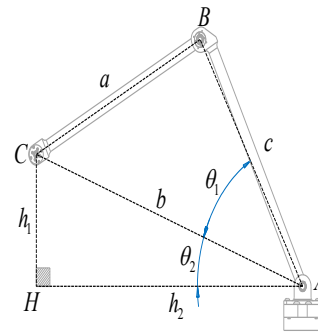

Fig. 2. Geometric interpretation of Remark 1.

$$M = s(n-j-1) + \sum_{i=1}^{j} \lambda_i = 6(11-12-1) + \sum_{i=1}^{12} 1 = 0 \qquad (1)$$

where M is the mobility, s denotes the mobility of an unconstrained body (six for spatial kinematic chains), n represents the number of bodies in the mechanism, j is the number of joints, and, finally, λ_i indicates the number of degrees of freedom allowed by the ith joint. Since there are eleven bodies and twelve 1-DOF joints (3 P-joints and 9 R-joints) in the Tripteron, the above formula results in $M = 0$. Thus, the Tripteron is indeed an over-constrained manipulator.

3- Kinematic Analysis

Prior to solving the kinematic equations, the following remark is stated, which will be needed further on:

Remark 1. As shown in Fig. 2, A, B and C are the vertices of an arbitrary triangle and ΔAHC is a right triangle ($A\hat{H}C = 90°$) with h_1 and h_2 edges. Then, $B\hat{A}H$ angle can be calculated as follows.

By writing the law of cosines for ΔABC, $\hat{\theta}_1$ and $\hat{\theta}_2$ can be expressed as:

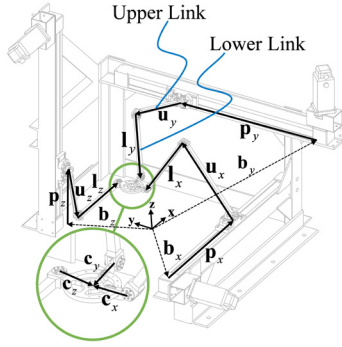$$\hat{\theta}_1 = \cos^{-1}\left(\frac{b^2 + c^2 - a^2}{2bc}\right). \qquad (2)$$

Fig. 3. Vector notation for the kinematic modeling of the Tripteron.

$$\hat{\theta}_2 = \tan^{-1}\left(\frac{h_1}{h_2}\right). \tag{3}$$

Thus, $B\hat{A}H$ angle can be obtained from the following equation:

$$B\hat{A}H = \hat{\theta}_1 + \hat{\theta}_2 = \cos^{-1}\left(\frac{b^2+c^2-a^2}{2bc}\right) + \tan^{-1}\left(\frac{h_1}{h_2}\right). \tag{4}$$

3- 1- Position analysis

As shown in Fig. 3, the origin of the world coordinate system is connected to each prismatic actuator guide-way's base point by the vector **b**. The position of the center of each prismatic actuator from the guide-way's base line is denoted by **p**. Furthermore, **u** and **l** are vectors along and equal to upper and lower link of each arm, respectively, and **c** is the vector connecting the revolute joint attached to the end-effector to its reference point. In what follows, the position, velocity, and acceleration of different parts of Tripteron are derived in terms of the position, velocity, and acceleration of the end-effector.

3- 2- Inverse displacement analysis

The vector representation of the manipulator under study is depicted in Fig. 3. Suppose that the position of the end-effector is denoted by $\mathbf{r}=\begin{bmatrix}X & Y & Z\end{bmatrix}^{\text{T}}$. Here, a vector loop closure equation can be written for the limb corresponding to the x-prismatic joint as follows:

$$\mathbf{b}_x + \mathbf{p}_x + \mathbf{u}_x + \mathbf{l}_x + \mathbf{c}_x = \begin{bmatrix}X & Y & Z\end{bmatrix}^{\text{T}}. \tag{5}$$

According to the fact that $\mathbf{p}_x$ is along the x-direction, $\mathbf{u}_x$, $\mathbf{l}_x$ and $\mathbf{c}_x$ are perpendicular to the x-direction. Taking the dot products of both sides of Eq.(5) with $\hat{i}$, the position of the x-prismatic joint can be expressed as:

$$\mathbf{p}_x = (X - \mathbf{b}_x.\hat{i})\hat{i}. \tag{6}$$

Inserting Eq.(6) into Eq.(5) leads to:

$$\lambda_x = \mathbf{u}_x + \mathbf{l}_x, \tag{7}$$

where λ_x can be obtained as:

$$\lambda_x = \begin{bmatrix}0 & Y & Z\end{bmatrix}^{\text{T}} - \mathbf{b}_x - \mathbf{c}_x + (\mathbf{b}_x.\hat{i})\hat{i}. \tag{8}$$

Refer to Remark 1. By substituting c with $\|\mathbf{u}_x\|$, a with $\|\mathbf{l}_x\|$, b with $\|\lambda_x\|$, h_1 with $Z - \mathbf{b}_x.\hat{k}$, and h_2 with $Y - (\mathbf{b}_x + \mathbf{c}_x).\hat{j}$, the angle between $\mathbf{u}_x$ and the y-axis can be written as follows:

$$\alpha_x = \cos^{-1}\left(\frac{\|\lambda_x\|^2 + \|\mathbf{u}_x\|^2 - \|\mathbf{l}_x\|^2}{2\|\mathbf{u}_x\|\|\lambda_x\|}\right) + \tan^{-1}\left(\frac{Z - \mathbf{b}_x.\hat{k}}{Y - (\mathbf{b}_x + \mathbf{c}_x).\hat{j}}\right). \tag{9}$$

Thus, having computed α_x, one can obtain $\mathbf{u}_x$ as:

$$\mathbf{u}_x = u_x(\cos\alpha_x\hat{j} + \sin\alpha_x\hat{k}), \tag{10}$$

and the vector $\mathbf{l}_x$ can be obtained by inserting Eq.(10) into Eq.(7):

$$\mathbf{l}_x = \lambda_x - u_x(\cos\alpha_x\hat{j} + \sin\alpha_x\hat{k}) \tag{11}$$

Similarly, considering the fact that $\mathbf{p}_y$ and $\mathbf{p}_z$ are respectively along the y- and z- directions, by taking the dot products of both sides of Eq.(5) with $\hat{j}$ and $\hat{k}$, the position of the y- and z-prismatic joints can be expressed as:

$$\mathbf{p}_y = (Y - \mathbf{b}_y.\hat{j})\hat{j} \tag{12}$$

$$\mathbf{p}_z = (Z - \mathbf{b}_z.\hat{k})\hat{k} \tag{13}$$

By Inserting Eqs.(12) and (13) into Eq.(5) and considering Remark 1, one can obtain $\mathbf{u}_y$ and $\mathbf{u}_z$ as:

$$\mathbf{u}_y = u_y(-\cos\alpha_y\hat{i} + \sin\alpha_y\hat{k}), \tag{14}$$

$$\mathbf{u}_z = u_z(-\cos\alpha_z\hat{j} - \sin\alpha_z\hat{i}), \tag{15}$$

where α_y and α_z are:

$$\alpha_y = \cos^{-1}\left(\frac{\|\lambda_y\|^2 + u_y^2 - l_y^2}{2u_y\|\lambda_y\|}\right) + \tan^{-1}\left(\frac{Z - \mathbf{b}_y.\hat{k}}{\mathbf{b}_y.\hat{i} - X}\right), \tag{16}$$

$$\alpha_z = \cos^{-1}\left(\frac{\|\lambda_z\|^2 + u_z^2 - l_z^2}{2u_z\|\lambda_z\|}\right) + \tan^{-1}\left(\frac{\mathbf{b}_z.\hat{i} - X}{\mathbf{b}_z.\hat{j} - Y}\right). \tag{17}$$

The variables λ_y and λ_z are defined as:

$$\lambda_y = \begin{bmatrix}X & 0 & Z\end{bmatrix}^{\text{T}} - \mathbf{b}_y + (\mathbf{b}_y.\hat{j})\hat{j}, \tag{18}$$

$$\lambda_z = \begin{bmatrix}X & Y & 0\end{bmatrix}^{\text{T}} - \mathbf{b}_z + (\mathbf{b}_z.\hat{k})\hat{k}. \tag{19}$$

Furthermore, by inserting Eqs.(14) and (15) into Eq.(17), one can obtain:

$$\mathbf{l}_y = \lambda_y - u_y(\cos\alpha_y\hat{j} + \sin\alpha_y\hat{k}), \tag{20}$$

$$\mathbf{l}_z = \lambda_z - u_z(\cos\alpha_z\hat{j} + \sin\alpha_z\hat{k}). \tag{21}$$

3- 3- Invese velocity analysis

Let $\mathbf{v}_{EE} = \begin{bmatrix}\dot{X} & \dot{Y} & \dot{Z}\end{bmatrix}^{\text{T}}$ be the vector of the output velocities of the end-effector. Taking the derivative of Eq.(5) with respect to time and knowing that $\dot{\mathbf{u}}_x = \omega_{ux}(\hat{i}\times\mathbf{u}_x)$ and $\dot{\mathbf{l}}_x = \omega_{lx}(\hat{i}\times\mathbf{l}_x)$ yields:

$$\begin{bmatrix}\dot{X} & \dot{Y} & \dot{Z}\end{bmatrix}^{\text{T}} = \dot{p}_x\hat{i} + \omega_{ux}(\hat{i}\times\mathbf{u}_x) + \omega_{lx}(\hat{i}\times\mathbf{l}_x), \tag{22}$$

where ω_{ux} and ω_{lx} are the magnitudes of the angular velocity of the x-upper link and the x-lower link, respectively. Dot product of both sides of Eq.(22) with $\hat{i}$, $\mathbf{l}_x$ and $\mathbf{u}_x$, will respectively lead to the following three equations:

$$\dot{p}_x = \dot{X}, \tag{23}$$

$$\omega_{ux} = \frac{\begin{bmatrix}0 & \dot{Y} & \dot{Z}\end{bmatrix}^{\text{T}}.\mathbf{l}_x}{(\hat{i}\times\mathbf{u}_x).\mathbf{l}_x}\hat{i}, \tag{24}$$

$$\omega_{lx} = \frac{\begin{bmatrix}0 & \dot{Y} & \dot{Z}\end{bmatrix}^{\text{T}}.\mathbf{u}_x}{(\hat{i}\times\mathbf{l}_x).\mathbf{u}_x}\hat{i}. \tag{25}$$

Since Eq.(22) is also valid for the y and z axes, dot product of both sides of Eq.(22) with $\hat{j}$ and $\hat{k}$ yields:

$$\dot{p}_y = \dot{Y} \tag{26}$$

$$\dot{p}_z = \dot{Z} \tag{27}$$

Also, dot product of both sides of Eq.(22) with $\mathbf{l}_y$ and $\mathbf{l}_z$ gives:

$$\omega_{uy} = \frac{[\dot{X} \quad 0 \quad \dot{Z}]^{\mathrm{T}}.\mathbf{l}_y}{(\hat{j} \times \mathbf{u}_y).\mathbf{l}_y}\hat{j}, \tag{28}$$

$$\omega_{uz} = \frac{[\dot{X} \quad \dot{Y} \quad 0]^{\mathrm{T}}.\mathbf{l}_z}{(\hat{k} \times \mathbf{u}_z).\mathbf{l}_z}\hat{k}. \tag{29}$$

Finally, by taking the dot product of both sides of Eq.(22) with $\mathbf{u}_y$ and $\mathbf{u}_z$, the following relations can be obtained:

$$\omega_{ly} = \frac{[\dot{X} \quad 0 \quad \dot{Z}]^{\mathrm{T}}.\mathbf{u}_y}{(\hat{j} \times \mathbf{l}_y).\mathbf{u}_y}\hat{j}, \tag{30}$$

$$\omega_{lz} = \frac{[\dot{X} \quad \dot{Y} \quad 0]^{\mathrm{T}}.\mathbf{u}_z}{(\hat{k} \times \mathbf{l}_z).\mathbf{u}_z}\hat{k}. \tag{31}$$

3- 4- Inverse acceleration analysis

For the dynamical modeling of the present manipulator, one should determine the acceleration vectors in the center of masses of the links. Assume that the acceleration of the end-effector is $\mathbf{a}_{EE} = [\ddot{X} \quad \ddot{Y} \quad \ddot{Z}]^{\mathrm{T}}$. Taking the time derivative of Eq.(22) with respect to time and knowing that $\ddot{\mathbf{u}} = \dot{\omega}_{ux}(\hat{i} \times \mathbf{u}_x) - \omega_{ux}^2 \mathbf{u}_x$ and $\ddot{\mathbf{l}}_x = \dot{\omega}_{lx}(\hat{i} \times \mathbf{l}_x) - \omega_{lx}^2 \mathbf{l}_x$ yield:

$$[\ddot{X} \quad \ddot{Y} \quad \ddot{Z}]^{\mathrm{T}} = \ddot{p}_x \hat{i} + \left(\dot{\omega}_{ux}(\hat{i} \times \mathbf{u}_x) - \omega_{ux}^2 \mathbf{u}_x\right) + \left(\dot{\omega}_{lx}(\hat{i} \times \mathbf{l}_x) - \omega_{lx}^2 \mathbf{l}_x\right). \tag{32}$$

Taking the inner product of both sides of Eq.(32) with $\hat{i}$ gives the linear acceleration of the prismatic actuators as follows:

$$\ddot{p}_x = \ddot{X}. \tag{33}$$

The inner product of Eq.(32) with $\mathbf{l}_x$ and $\mathbf{u}_x$ leads to the following equations:

$$\dot{\omega}_{ux} = \frac{\omega_{ux}^2 \mathbf{u}_x.\mathbf{l}_x + \omega_{lx}^2 \mathbf{l}_x.\mathbf{l}_x + [0 \quad \ddot{Y} \quad \ddot{Z}]^{\mathrm{T}}.\mathbf{l}_x}{(\hat{i} \times \mathbf{u}_x).\mathbf{l}_x}, \tag{34}$$

$$\dot{\omega}_{lx} = \frac{\omega_{ux}^2 \mathbf{u}_x.\mathbf{u}_x + \omega_{lx}^2 \mathbf{l}_x.\mathbf{u}_x + [0 \quad \ddot{Y} \quad \ddot{Z}]^{\mathrm{T}}.\mathbf{u}_x}{(\hat{i} \times \mathbf{l}_x).\mathbf{u}_x}. \tag{35}$$

Assume that the distance of the center of mass of the x-upper link from the revolute joint connected to its corresponding prismatic actuator is $\gamma_{ux} u_x$ and the distance of the center of mass of the x-lower link from the revolute joint connected to the x-upper link is $\gamma_{lx} l_x$. The accelerations of the center of mass of the x-upper link, $\mathbf{a}_{ux}$, and the x-lower link, $\mathbf{a}_{lx}$, can be respectively obtained from:

$$\mathbf{a}_{ux} = \ddot{p}_x \hat{i} + \gamma_{ux} u_x \left(\dot{\omega}_{ux}(\hat{i} \times \mathbf{u}_x) - \omega_{ux}^2 \mathbf{u}_x\right), \tag{36}$$

$$\mathbf{a}_{lx} = \ddot{p}_x \hat{i} + \tilde{a}_{lx} l_x \left(\dot{\omega}_{lx}(\hat{i} \times \mathbf{l}_x) - \omega_{lx}^2 \mathbf{l}_x\right) - \omega_{ux}^2 \mathbf{u}_x + \dot{\omega}_{ux}(\hat{i} \times \mathbf{u}_x). \tag{37}$$

Since Eq.(32) is also valid for the y and z axes, the same methodology to assess the kinematic characteristics of the other links has been applied. Taking the inner product of both sides of Eq.(32) with $\hat{j}$ and $\hat{k}$ attains the linear accelerations of the y and z prismatic actuators as:

$$\ddot{p}_y = \ddot{Y} \tag{38}$$

$$\ddot{p}_z = \ddot{Z} \tag{39}$$

Inner product of Eq.(32) with $\mathbf{l}_y$ and $\mathbf{l}_z$ leads to the following equations:

$$\dot{\omega}_{uy} = \frac{\omega_{uy}^2 \mathbf{u}_y.\mathbf{l}_y + \omega_{ly}^2 \mathbf{l}_y.\mathbf{l}_y + [\ddot{X} \quad 0 \quad \ddot{Z}]^{\mathrm{T}}.\mathbf{l}_y}{(\hat{j} \times \mathbf{u}_y).\mathbf{l}_y} \tag{40}$$

$$\dot{\omega}_{uz} = \frac{\omega_{uz}^2 \mathbf{u}_z.\mathbf{l}_z + \omega_{lz}^2 \mathbf{l}_z.\mathbf{l}_z + [\ddot{X} \quad \ddot{Y} \quad 0]^{\mathrm{T}}.\mathbf{l}_z}{(\hat{k} \times \mathbf{u}_z).\mathbf{l}_z} \tag{41}$$

Furthermore, the inner product of Eq.(32) with $\mathbf{u}_y$ and $\mathbf{u}_z$ leads to:

$$\dot{\omega}_{ly} = \frac{\omega_{uy}^2 \mathbf{u}_y.\mathbf{u}_y + \omega_{ly}^2 \mathbf{l}_y.\mathbf{u}_y + [\ddot{X} \quad 0 \quad \ddot{Z}]^{\mathrm{T}}.\mathbf{u}_y}{(\hat{j} \times \mathbf{l}_y).\mathbf{u}_y} \tag{42}$$

$$\dot{\omega}_{lz} = \frac{\omega_{uz}^2 \mathbf{u}_z.\mathbf{u}_z + \omega_{lz}^2 \mathbf{l}_z.\mathbf{u}_z + [\ddot{X} \quad \ddot{Y} \quad 0]^{\mathrm{T}}.\mathbf{u}_z}{(\hat{k} \times \mathbf{l}_z).\mathbf{u}_z} \tag{43}$$

Assume that the distance of the center of mass of the y- and z-upper links from the revolute joint connected to their corresponding prismatic actuators are respectively $\gamma_{uy} u_y$ and $\gamma_{uz} u_z$, and the distance of the center of mass of the y- and z-lower link from their revolute joints are $\gamma_{ly} l_y$ and $\gamma_{lz} l_z$, respectively. The acceleration of the center of mass of the y- and z-upper links, and the y- and z-lower links, can be respectively obtained as:

$$\mathbf{a}_{uy} = \ddot{p}_y \hat{j} + \gamma_{uy} u_y \left(\dot{\omega}_{uy}(\hat{j} \times \mathbf{u}_y) - \omega_{uy}^2 \mathbf{u}_y\right), \tag{44}$$

$$\mathbf{a}_{ly} = \ddot{p}_y \hat{j} + \gamma_{ly} l_y \left(\dot{\omega}_{ly}(\hat{j} \times \mathbf{l}_y) - \omega_{ly}^2 \mathbf{l}_y\right) - \omega_{uy}^2 \mathbf{u}_y + \dot{\omega}_{uy}(\hat{j} \times \mathbf{u}_y), \tag{45}$$

$$\mathbf{a}_{uz} = \ddot{p}_z \hat{k} + \gamma_{uz} u_z \left(\dot{\omega}_{uz}(\hat{k} \times \mathbf{u}_z) - \omega_{uz}^2 \mathbf{u}_z\right), \tag{46}$$

$$\mathbf{a}_{lz} = \ddot{p}_z \hat{k} + \gamma_{lz} l_z \left(\dot{\omega}_{lz}(\hat{k} \times \mathbf{l}_z) - \omega_{lz}^2 \mathbf{l}_z\right) - \omega_{uz}^2 \mathbf{u}_z + \dot{\omega}_{uz}(\hat{k} \times \mathbf{u}_z). \tag{47}$$
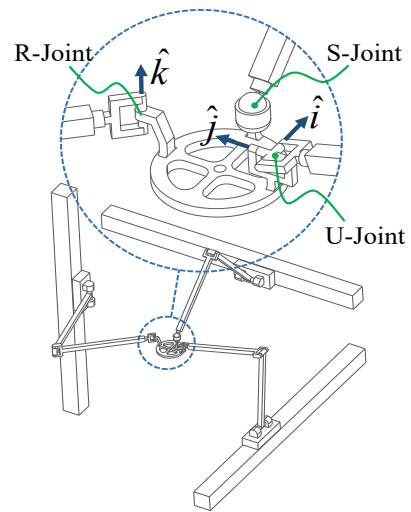
4- Dynamic Analysis

Fig. 4. The modified fully-constrained manipulator.

As aforementioned, the manipulator is an over-constraint manipulator. Thus, in order to solve the dynamical model through Newton-Euler approach, one should lessen the

dynamical constraints of the manipulator by replacing some of the joints with ones with more DO, without changing the overall kinematic constraints imposed to the end-effector. In this paper, in order to equalize the number of equations and the number of the unknowns, as shown in Fig. 4, the revolute joints connecting the end-effector to the lower links associated with the y- and x- limbs are replaced by a spherical and a universal joint, respectively. Now, by using the Chebychev–Grübler–Kutzbach formula for the mobility of the modified mechanism, one obtains $M = 3$, which says that the modified 3-DOF mechanism has been determined. In Fig. 5, the forces and moments applied to the links of the modified manipulator are shown. In the latter figure, $\mathbf{F}_{LxEE}$ and $\mathbf{M}_{LxEE}$ are respectively the reaction force and moment of the x-lower link, acting on the end-effector. Also, $\mathbf{F}_{UxLx}$ and $\mathbf{M}_{UxLx}$ are respectively the reaction force and moment of the x-upper link, acting on the x-lower link. The x-lower link is also subjected to the gravitational force, that is $-m_{lx}g\hat{k}$, at its center of mass. Establishing all the external force and moment components on the x-lower link and balancing the moment components around the revolute joint connecting the lower link to the upper link give:

$$-\mathbf{l}_x \times \mathbf{F}_{lxEE} + \mathbf{M}_{UxLx} - \mathbf{M}_{LxEE} = m_{lx}\gamma_{lx}\mathbf{l}_x \times (\mathbf{a}_{lx} + g\hat{k}) + \dot{\mathbf{H}}_{lx}, \quad (48)$$
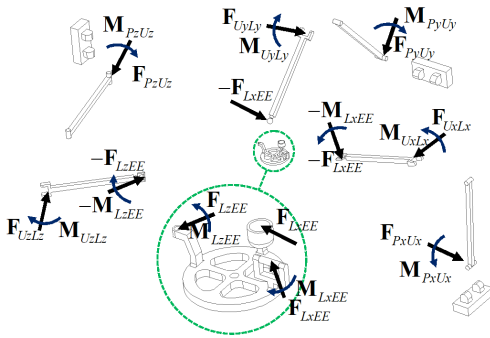

Fig. 5. Free-body diagram of the understudy manipulator after dynamical constraint reduction.

where $\mathbf{H}_{lx}$ is the angular momentum of the x-lower link around its center of mass. By considering the fact that x-lower link only rotates along x-direction, $\dot{\mathbf{H}}_{lx}$ can be written as:

$$\dot{\mathbf{H}}_{lx} = I_{lx}\dot{\omega}_{lx}\hat{i}, \quad (49)$$

where I_{lx} represents the mass moment of inertia along the direction normal to the x-lower link at its center of mass. Since $\mathbf{M}_{UxLx}$ and $\mathbf{M}_{LxEE}$ do not have any component along the $\hat{i}$ direction, by taking the dot product of both sides of Eq. (48) with $\hat{i}$, one has:

$$(\mathbf{l}_x \times \hat{i}).\mathbf{F}_{LxEE} = m_{lx}\gamma_{lx}(\hat{i} \times \mathbf{l}_x).(\mathbf{a}_{lx} + g\hat{k}) + I_{lx}\dot{\omega}_{lx}. \quad (50)$$

In Fig. 5, $\mathbf{F}_{PxUx}$ and $\mathbf{M}_{PxUx}$ are respectively the reaction force and moment of the x-prismatic joint acting on the x-upper link; balancing the moment components around the revolute joint attached to the x-prismatic joint results in:

$$\mathbf{M}_{PxUx} - \mathbf{M}_{LxEE} - (\mathbf{l}_x + \mathbf{u}_x) \times \mathbf{F}_{LxEE} =$$
$$(I_{lx}\dot{\omega}_{lx} + I_{ux}\dot{\omega}_{ux})\hat{i} + m_{lx}(\gamma_{lx}\mathbf{l}_x + \mathbf{u}_x) \times (\mathbf{a}_{lx} + g\hat{k}) \quad (51)$$
$$+ m_{ux}\gamma_{ux}\mathbf{u}_x \times (\mathbf{a}_{ux} + g\hat{k}).$$

Since $\mathbf{M}_{UxLx}$ and $\mathbf{M}_{LxEE}$ do not have any component along $\hat{i}$ direction, by taking the dot product of both sides of the latter equation with $\hat{i}$, and using the general formula of $\mathbf{a}.(\mathbf{b} \times \mathbf{c}) = \mathbf{b}.(\mathbf{c} \times \mathbf{a}) = \mathbf{c}.(\mathbf{a} \times \mathbf{b})$, the following could be obtained:

$$((\mathbf{l}_x + \mathbf{u}_x) \times \hat{i}).\mathbf{F}_{LxEE} = (\hat{i} \times (\gamma_{lx}\mathbf{l}_x + \mathbf{u}_x)).(m_{lx}(\mathbf{a}_{lx} + g\hat{k}))$$
$$+ I_{lx}\dot{\omega}_{lx} + I_{ux}\dot{\omega}_{ux} + m_{ux}\gamma_{ux}(\hat{i} \times \mathbf{u}_x).(\mathbf{a}_{ux} + g\hat{k}). \quad (52)$$

Now, in order to obtain $\mathbf{F}_{LxEE}$, $\mathbf{F}_{LxEE}$ is projected into three components, first component F_{LxEE}^x along the x-direction, second component F_{LxEE}^a along the axis of the x-lower link, and third component F_{LxEE}^n normal to the plane containing the axis of the x-lower link and the x-direction. By using the latter assumption, one can write $\mathbf{F}_{LxEE}$ as:

$$\mathbf{F}_{LxEE} = F_{LxEE}^x\hat{i} + F_{LxEE}^a\mathbf{e}_{lx} + F_{LxEE}^n(\hat{i} \times \mathbf{e}_{lx}), \quad (53)$$

where $\mathbf{e}_{lx}$ is the unit vector in $\mathbf{l}_x$ direction. With a similar decomposition, $\mathbf{F}_{LyEE}$ and $\mathbf{F}_{LzEE}$ are obtained:

$$\mathbf{F}_{LyEE} = F_{LyEE}^y\hat{j} + F_{LyEE}^a\mathbf{e}_{ly} + F_{LyEE}^n(\hat{j} \times \mathbf{e}_{ly}), \quad (54)$$

$$\mathbf{F}_{LzEE} = F_{LzEE}^z\hat{k} + F_{LzEE}^a\mathbf{e}_{lz} + F_{LzEE}^n(\hat{k} \times \mathbf{e}_{lz}), \quad (55)$$

where $\mathbf{e}_{ly}$ and $\mathbf{e}_{lz}$ are the unit vectors in $\mathbf{l}_y$ and $\mathbf{l}_z$ directions. Inserting Eq.(53) into Eqs.(50) and (52) yields the following equations:

$$F_{LxEE}^n = m_{lx}\gamma_{lx}(\mathbf{e}_{lx} \times \hat{i}).(\mathbf{a}_{lx} + g\hat{k}) - \frac{I_{lx}\dot{\omega}_{lx}}{l_x}, \quad (56)$$

$$F_{LxEE}^a = m_{ux}\gamma_{ux}\frac{(\hat{i} \times \mathbf{u}_x).(\mathbf{a}_{ux} + g\hat{k})}{(\mathbf{e}_x \times \mathbf{u}_x).\hat{i}}$$
$$- \frac{\dot{\omega}_{lx}I_{lx}l_x\mathbf{u}_x.\mathbf{e}_x + \dot{\omega}_{ux}I_{ux}}{(\mathbf{e}_x \times \mathbf{u}_x).\hat{i}} + \frac{\dot{\omega}_{ux}I_{ux}}{(\mathbf{e}_x \times \mathbf{u}_x).\hat{i}}$$
$$+ \frac{m_{lx}\hat{i} \times (\mathbf{u}_x - \gamma_{lx}(\mathbf{u}_x.\mathbf{e}_x)\mathbf{e}_x)}{(\mathbf{e}_x \times \mathbf{u}_x).\hat{i}}.(\mathbf{a}_{lx} + g\hat{k}). \quad (57)$$

By appying a similar procedure for the y and z limbs, the following results are obtained:

$$F_{LyEE}^n = m_{ly}\gamma_{ly}(\mathbf{e}_{ly} \times \hat{j}).(\mathbf{a}_{ly} + g\hat{k}) - \frac{I_{ly}\dot{\omega}_{ly}}{l_y}, \quad (58)$$

$$F_{LzEE}^n = m_{lz}\gamma_{lz}(\mathbf{e}_{lz} \times \hat{k}).\mathbf{a}_{lz} - \frac{I_{lz}\dot{\omega}_{lz}}{l_z}, \quad (59)$$

$$F_{LyEE}^a = m_{uy}\gamma_{uy}\frac{(\hat{j} \times \mathbf{u}_y).(\mathbf{a}_{uy} + g\hat{k})}{(\mathbf{e}_y \times \mathbf{u}_y).\hat{j}} - \frac{\dot{\omega}_{ly}I_{ly}l_y\mathbf{u}_y.\mathbf{e}_y + \dot{\omega}_{uy}I_{uy}}{(\mathbf{e}_y \times \mathbf{u}_y).\hat{j}}$$
$$+ \frac{m_{ly}\hat{j} \times (\mathbf{u}_y - \gamma_{ly}(\mathbf{u}_y.\mathbf{e}_y)\mathbf{e}_y)}{(\mathbf{e}_y \times \mathbf{u}_y).\hat{j}}.(\mathbf{a}_{ly} + g\hat{k}), \quad (60)$$

$$F_{LzEE}^a = m_{uz}\gamma_{uz}\frac{(\hat{k} \times \mathbf{u}_z).\mathbf{a}_{uz}}{(\mathbf{e}_z \times \mathbf{u}_z).\hat{k}} - \frac{\dot{\omega}_{lz}I_{lz}l_z\mathbf{u}_z.\mathbf{e}_z + \dot{\omega}_{uz}I_{uz}}{(\mathbf{e}_z \times \mathbf{u}_z).\hat{k}}$$
$$+ \frac{m_{lz}\hat{k} \times (\mathbf{u}_z - \gamma_{lz}(\mathbf{u}_z.\mathbf{e}_z)\mathbf{e}_z)}{(\mathbf{e}_z \times \mathbf{u}_z).\hat{k}}.\mathbf{a}_{lz}. \quad (61)$$

According to Fig. 5, after imposing the external force and moment vectors on the end-effector and writing the force equilibrium equation for the end-effector, the following is obtained:

$$\mathbf{F}_{LxEE} + \mathbf{F}_{LyEE} + \mathbf{F}_{LzEE} = m_{EE}\begin{bmatrix} \ddot{X} & \ddot{Y} & \ddot{Z} \end{bmatrix}^{\mathrm{T}}. \qquad (62)$$

Inserting Eqs.(53),(54) and (55) into Eq.(62), yields:

$$m_{EE}\begin{bmatrix} \ddot{X} & \ddot{Y} & \ddot{Z} \end{bmatrix}^{\mathrm{T}} = F_{LxEE}^{x}\hat{i} + F_{LyEE}^{y}\hat{j} + F_{LzEE}^{z}\hat{k} + F_{LxEE}^{a}\mathbf{e}_{lx}$$
$$+ F_{LyEE}^{a}\mathbf{e}_{ly} + F_{LzEE}^{a}\mathbf{e}_{lz} + F_{LxEE}^{n}(\hat{i}\times\mathbf{e}_{lx}) \qquad (63)$$
$$+ F_{LyEE}^{n}(\hat{j}\times\mathbf{e}_{ly}) + F_{LzEE}^{n}(\hat{k}\times\mathbf{e}_{lz}).$$

The inner product of Eq.(63) by $\hat{i}$, $\hat{j}$ and $\hat{k}$ respectively results in:

$$F_{LxEE}^{x} = m_{EE}\ddot{X} + F_{LzEE}^{n}(\hat{j}\times\mathbf{e}_{lz}) - F_{LyEE}^{a}(\mathbf{e}_{ly}.\hat{i})$$
$$- F_{LzEE}^{a}(\mathbf{e}_{lz}.\hat{i}) - F_{LyEE}^{n}(\hat{k}.\mathbf{e}_{ly}), \qquad (64)$$

$$F_{LyEE}^{y} = m_{EE}\ddot{Y} + F_{LxEE}^{n}(\hat{k}\times\mathbf{e}_{lx}) - F_{LxEE}^{a}(\mathbf{e}_{lx}.\hat{j})$$
$$- F_{LzEE}^{a}(\mathbf{e}_{lz}.\hat{j}) - F_{LzEE}^{n}(\hat{i}.\mathbf{e}_{lz}), \qquad (65)$$

$$F_{LzEE}^{z} = m_{EE}\ddot{Z} + F_{LyEE}^{n}(\hat{i}.\mathbf{e}_{ly}) - F_{LxEE}^{a}(\mathbf{e}_{lx}.\hat{k})$$
$$- F_{LyEE}^{a}(\mathbf{e}_{ly}.\hat{k}) - F_{LxEE}^{n}(\hat{j}.\mathbf{e}_{lx}). \qquad (66)$$

Now, by applying Newton's second law to the *x*-limb, the total force that is acting on the prismatic joint is obtained from:

$$\mathbf{F}_{px} = \mathbf{F}_{LxEE} + m_{lx}\mathbf{a}_{lx} + m_{ux}\mathbf{a}_{ux} + m_{px}\ddot{p}_{x}\hat{i}$$
$$+ (m_{lx} + m_{ux} + m_{px})g\hat{k}. \qquad (67)$$

The force that the actuator of the *x*-limb exerts on the platform is given by taking the dot product of Eq. (67) by $\hat{i}$ and is as follows:

$$\mathbf{F}_{px}.\hat{i} = F_{LxEE}^{x} + m_{lx}\mathbf{a}_{lx}.\hat{i} + m_{ux}\mathbf{a}_{ux}.\hat{i} + m_{px}\ddot{p}_{x}. \qquad (68)$$

By following a similar procedure for the *y* and *z* limb, the following results can be obtained:

$$\mathbf{F}_{py}.\hat{j} = F_{LyEE}^{y} + m_{ly}\mathbf{a}_{ly}.\hat{j} + m_{uy}\mathbf{a}_{uy}.\hat{j} + m_{py}\ddot{p}_{y}, \qquad (69)$$

$$\mathbf{F}_{pz}.\hat{k} = F_{LzEE}^{z} + m_{lz}\mathbf{a}_{lz}.\hat{k} + m_{uz}\mathbf{a}_{uz}.\hat{k}$$
$$+ m_{pz}\ddot{p}_{z} + (m_{lz} + m_{uz} + m_{pz})g. \qquad (70)$$

5- Model Validation and Discussion

In order to verify the performance of the proposed mathematical dynamical model of the manipulator, a simulation study is performed in this section, and the obtained results from the mathematical model will be compared with the corresponding results of the SimMechanics model. Actuation and joint forces and torques are calculated for both phases and are compared to understand the dynamic requirements in the joints and links of the manipulator. In the simulation, the physical parameters of the manipulator are obtained according to the CAD model and are given in Table 1. The mass of the end-effector is assumed to be $m_{EE} = 0.75$ Kg and the gravity vector is taken as $-9.81\hat{k}$ m/s^2.

Table 1. Geometric and inertia properties of the manipulator.

	$i = x$	$i = y$	$i = z$
$\mathbf{b}_i$	[0 0.04 0.063]$^{\mathrm{T}}$	[0 0.04 0.063]$^{\mathrm{T}}$	[0 0.04 0.063]$^{\mathrm{T}}$
l_i	0.392	0.392	0.392
u_i	0.443	0.443	0.443
m_{li}	1.75	1.75	1.75
m_{ui}	2	2	2
γ_{ui}	0.5	0.5	0.5
γ_{li}	0.5	0.5	0.5
I_{li}	0.0224	0.0224	0.0224
I_{ui}	0.0327	0.0327	0.0327

* All of the parameters are in SI units.

In order to verify the accuracy of the proposed dynamical models by SimMechanics and experimental data, the forces related to the prismatic joints are studied which are shown in Fig. 7 with a solid green line. In order to obtain the experimental data, the Tripteron manipulator is driven by means of a PID controller to track a desired trajectory. The control action is applied with a frequency of 150 Hz. The internal encoder of each servo motor provides the joint positions, and the actuation torques are measured indirectly by means of the motors' current[1]. The measurements were taken with a frequency of 150 Hz. Since direct numerical differentiation of the measured joint angle yields noisy results, the determination of joint velocity and acceleration were carried out by fitting the measured joint angles to Fourier series as presented in [23]. In order to reduce the effect of noise in sampled measurements, trajectories were repeated several times and the measurements were averaged; then, a second order low pass digital Butterworth with a normalized cut of frequency of 5 Hz was applied. Also, in order to avoid phase distortion of the filtered signals, the `filtfilt` function of Matlab was used.

For the simulation study, the end-effector exhibits a sinusoidal motion along each direction. The motion of the end-effector is written below as a function of time:

$$\begin{cases} X = 0.7 + 0.1\sin(4t) \\ Y = 0.4 + 0.1\sin(2t) \\ Z = 0.2 + 0.1\sin(2t) \end{cases} \qquad (71)$$

---

[1] The relationship between the current and the torque was obtained through experiments that were conducted on the servo motors.
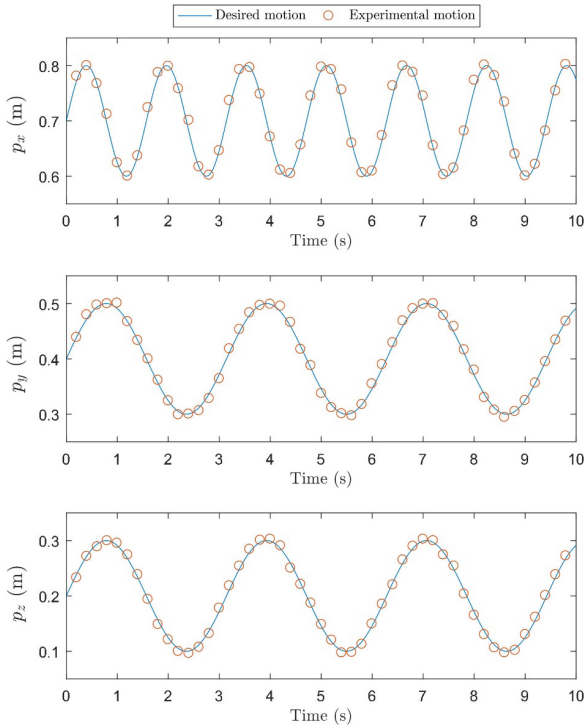
Fig. 6. Comparison between the experimental and simulated trajectories.
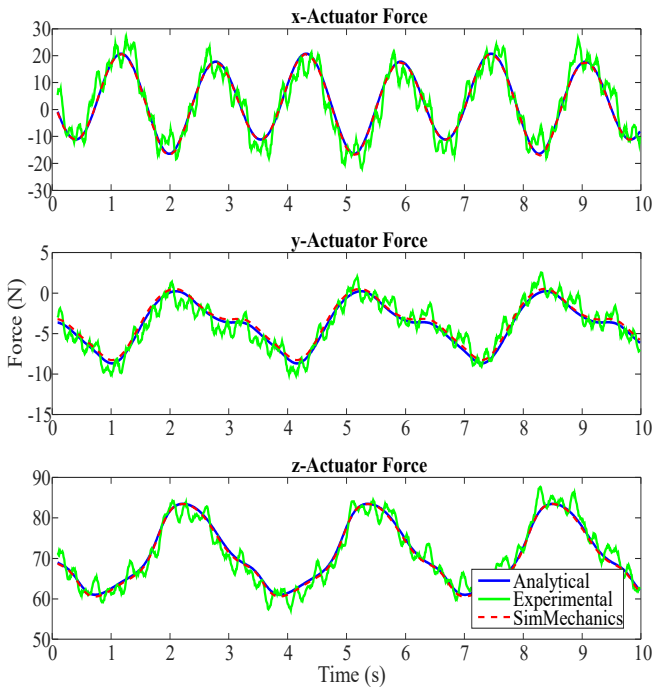

Fig. 7. Results of the experimental and simulation study for the motion presented in function (71).

Fig. 6 shows the comparison between the desired trajectory and the one tracked by the manipulators' actuated joints. From Fig. 7, it can be seen that the obtained results from the proposed model, SimMechanics, and experimental study are coherent which validate the correctness of the dynamic equations.

Table 2. RMSE for the results shown in Fig. 7 based on the analytical solution.

Model	RMSE
SimMechanics model	0.147
Experimental results	6.56

In order to validate the correctness of the analytical model for joint forces and torques, two diagrams are presented in Fig. 8 and Fig. 9 for the trajectory defined in function (71), which correspond to the internal forces between the upper link and prismatic joint (Fig. 8) and moments imposed by the upper link to the lower link (Fig. 9). It can be seen that the results derived by SimMechanics and those obtained from formulas are in a good agreement which confirms the correctness of the mathematical model.
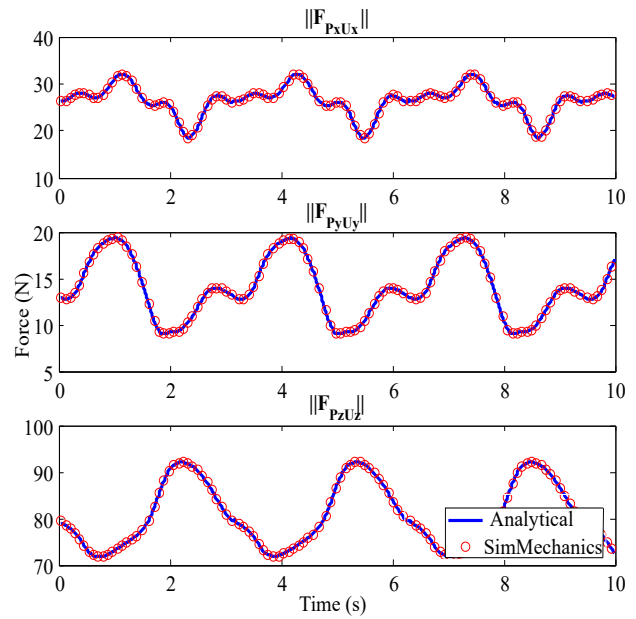

Fig. 8. Results of the analytical model and simulation study for the joint force between prismatic joint and upper link in each arm for the motion presented in function (71).
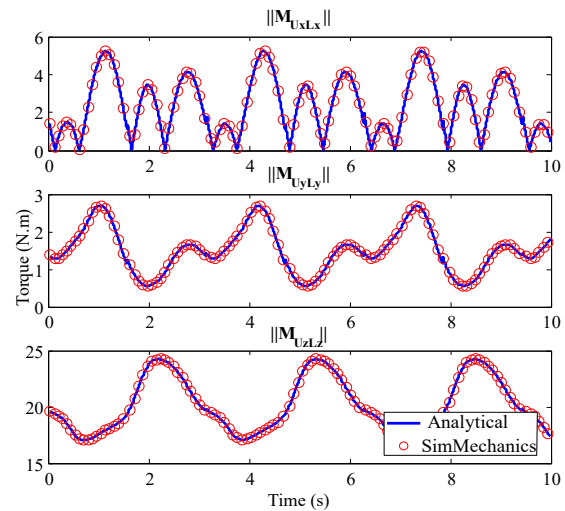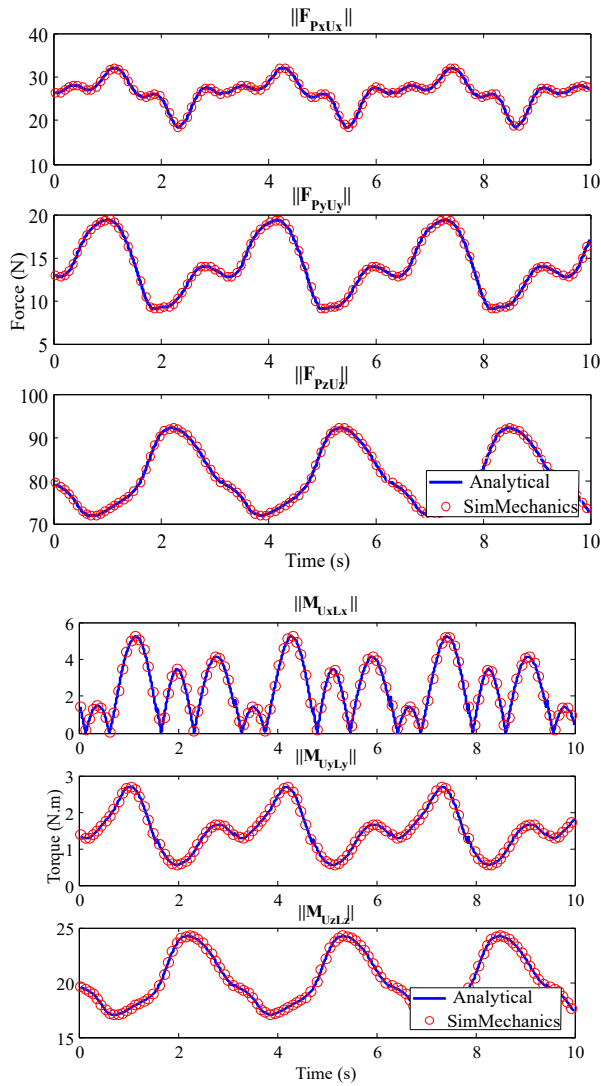

Fig. 9. Results of the analytical model and simulation study for the joint torque between upper links and lower links in each arm for the motion presented in function (71).

The Root Mean Square Error (RMSE) for the difference between the mathematical solution and the results from the SimMechanics model and practical data for this study are reported in Table 1. The difference between an analytical solution and the experimental result is mainly due to the friction force between the slider blocks and the guide rails.

The results of these two figures and several practical tests reveal that the torques and forces exerted to the links of the *z*-arm are significantly higher than those of the other links. It can be deduced that for designing such a manipulator, joints and links should be stronger in the *z*-arm since they bear higher torques and forces.

for the SimMechanics and experimental test were obtained at 0.147 and 6.56, respectively. We believe the present error between the experimental test and the analytical formula is due to two main factors: The friction between the prismatic joints and their guide rails, and the difference between the value of the inertial parameters used in the dynamical model and their actual value. Furthermore, the results provided some insights into the amount of force in passive joints and by performing several tests, it revealed that the joints and links corresponding to the *z*-direction undergo higher forces and torques which should be taken into account in the design stage. Ongoing work will includ stiffness analysis, modeling, and identification of the friction in order to make the model more accurate.

Nomenclature

$\mathbf{a}_{EE}$	The vector of acceleration of the end-effector
$\mathbf{a}_l$	The acceleration of the center of mass of the lower link
$\mathbf{c}$	The vector connecting the revolute joint attached to the end-effector to its reference point
$\mathbf{F}_U$	The reaction force of the upper link
$\mathbf{H}_l$	The angular momentum of the lower link around its mass center
$\mathbf{M}_U$	Reaction moment of the upper link
$\mathbf{p}$	The distance of the center of each prismatic actuator from the guide-way's base line
$\mathbf{u}$	The vector along and equal to upper link of the arm
α	The angle between upper link and the horizontal line
ω_l	The vector of the angular velocity of the lower link
$\mathbf{a}_u$	The acceleration of the center of mass of the upper link
$\mathbf{b}$	The vector that connects the world coordinate system to the prismatic actuator guide-way's base point
$\mathbf{F}_L$	The reaction force of the lower link
$\mathbf{F}_p$	The force exerted on the platform by the actuator
$\mathbf{l}$	The vector along and equal to lower link of the arm
$\mathbf{M}_L$	Reaction moment of the lower link
$\mathbf{r}$	The position of the end-effector in the world coordinate system
$\mathbf{v}_{EE}$	The vector of the output velocities of the end-effector
ω_u	The vector of the angular velocity of the upper link

6- Conclusion

This paper addressed the mathematical modeling of the kinematics and dynamics of a 3-DOF translational PM. The kinematics of a mechanism is defined via a vector-loop closure approach and all the expressions are expressed using vector notation which, afterward, made it possible to have a compact dynamics' formulation. The dynamical model of the manipulator was developed using Newton-Euler approach and a compact formulation was obtained for the first time. To illustrate the accuracy of the proposed dynamical model, a simulation study was performed for a given trajectory and the obtained results from the analytical formulas, SimMechanics model, and experimental tests were compared. The RMSE

References

[1] J.-P. Merlet, C. Gosselin, Parallel mechanisms and robots, in: Springer Handbook of Robotics, Springer, 2008, pp. 269-285.

[2] L.-W. Tsai, Robot analysis: the mechanics of serial and parallel manipulators, John Wiley & Sons, 1999

[3] M. Isaksson, T. Brogårdh, S. Nahavandi, Parallel manipulators with a rotation-symmetric arm system, Journal of mechanical design, 134(11) (2012) 114503.

[4] M. Isaksson, T. Brogårdh, M. Watson, S. Nahavandi, P. Crothers, The Octahedral Hexarot—A novel 6-DOF parallel manipulator, Mechanism and machine theory, 55 (2012) 91-102

[5] M. Isaksson, A. Eriksson, M. Watson, T. Brogårdh, S. Nahavandi, A method for extending planar axis-symmetric parallel manipulators to spatial mechanisms, Mechanism and Machine Theory, 83 (2015) 1-13

[6] C. Gosselin, Compact dynamic models for the tripteron and quadrupteron parallel manipulators, Proceedings of the Institution of Mechanical Engineers, Part I: Journal of Systems and Control Engineering, 223(1) (2009) 1-12

[7] B. Danaei, A. Arian, M.T. Masouleh, A. Kalhor, Kinematic and Dynamic Modeling and Base Inertial Parameters Determination of the Quadrupteron Parallel Manipulator, in: Computational Kinematics, Springer, (2018), pp. 249-256

[8] M.T. Masouleh, M.H. Saadatzi, C.m. Gosselin, H.D. Taghirad, A geometric constructive approach for the workspace analysis of symmetrical 5-PRUR parallel mechanisms (3T2R), in: ASME Design Engineering Technical Conferences, (2010), pp. 15-18

[9] C. Quennouelle, C. Gosselin, Kinematostatic modeling of compliant parallel mechanisms, Meccanica, 46(1) (2011) 155-169

[10] C.M. Gosselin, M.T. Masouleh, V. Duchaine, P.-L. Richard, S. Foucault, X. Kong, Parallel mechanisms of the multipteron family: kinematic architectures and benchmarking, in: Robotics and Automation, 2007 IEEE International Conference on, IEEE, (2007), pp. 555-560

[11] X. Kong, C.M. Gosselin, Kinematics and singularity analysis of a novel type of 3-CRR 3-DOF translational parallel manipulator, The International Journal of Robotics Research, 21(9) (2002) 791-798

[12] M. Sharifzadeh, M.T. Masouleh, A. Kalhor, On human–robot interaction of a 3-DOF decoupled parallel mechanism based on the design and construction of a novel and low-cost 3-DOF force sensor, Meccanica, 52(2017) 2471-2490

[13] R. Di Gregorio, V. Parenti-Castelli, Dynamics of a class of parallel wrists, in: ASME 2002 International Design Engineering Technical Conferences and Computers and Information in Engineering Conference, American Society of Mechanical Engineers, 2002, pp. 269-277

[14] Y. Li, Q. Xu, Dynamic modeling and robust control of a 3-PRC translational parallel kinematic machine, Robotics and Computer-Integrated Manufacturing, 25(3) (2009) 630-640

[15] B. Danaei, A. Arian, M.T. Masouleh, A. Kalhor, Dynamic modeling and base inertial parameters determination of a 2-DOF spherical parallel mechanism, Multibody System Dynamics, 41(4) (2017) 367-390

[16] H. Kalani, A. Rezaei, A. Akbarzadeh, Improved general solution for the dynamic modeling of Gough–Stewart platform based on principle of virtual work, Nonlinear Dynamics, 83(4) (2016) 2393-2418

[17] J. Wang, C.M. Gosselin, A new approach for the dynamic analysis of parallel manipulators, Multibody System Dynamics, 2(3) (1998) 317-334

[18] A. Arian, B. Danaei, M.T. Masouleh, Kinematics and dynamics analysis of a 2-DOF spherical parallel robot, in: Robotics and Mechatronics (ICROM), 2016 4th International Conference on, IEEE, 2016, pp. 154-159

[19] Z. Bi, S. Lang, M. Verner, Dynamic modeling and validation of a tripod-based machine tool, The International Journal of Advanced Manufacturing Technology, 37(3-4) (2008) 410-421

[20] Y.-W. Li, J.-S. Wang, L.-P. Wang, X.-J. Liu, Inverse dynamics and simulation of a 3-DOF spatial parallel manipulator, in: Robotics and Automation, 2003. Proceedings. ICRA'03. IEEE International Conference on, IEEE, 2003, pp. 4092-4097

[21] T.D. Thanh, J. Kotlarski, B. Heimann, T. Ortmaier, On the inverse dynamics problem of general parallel robots, in: Mechatronics, 2009. ICM 2009. IEEE International Conference on, IEEE, 2009, pp. 1-6

[22] W. Do, D. Yang, Inverse dynamic analysis and simulation of a platform type of robot, Journal of Robotic Systems, 5(3) (1988) 209-227

[23] C. Reboulet, T. Berthomieu, Dynamic models of a six degree of freedom parallel manipulators, in: Advanced Robotics, 1991.'Robots in Unstructured Environments', 91 ICAR., Fifth International Conference on, IEEE, 1991, pp. 1153-1157

[24] A.M. Lopes, Dynamic modeling of a Stewart platform using the generalized momentum approach, Communications in Nonlinear Science and Numerical Simulation, 14(8) (2009) 3389-3401

[25] E. Zahariev, J. Cuadrado, Dynamics of over-constrained rigid and flexible multibody systems, in: 12th IFToMM World Congress, Besançon, France, 2007

[26] D. Gan, J.S. Dai, J. Dias, L. Seneviratne, Joint force decomposition and variation in unified inverse dynamics analysis of a metamorphic parallel mechanism, Meccanica, 51(7) (2016) 1583-1593

[27] Z. Bi, B. Kang, An inverse dynamic model of over-constrained parallel kinematic machine based on Newton–Euler formulation, Journal of Dynamic Systems, Measurement, and Control, 136(4) (2014) 041001

[28] C. Gosselin, Parallel computational algorithms for the kinematics and dynamics of planar and spatial parallel manipulators, Journal of Dynamic Systems, Measurement, and Control, 118(1) (1996) 22-28

[29] X. Kong, C.M. Gosselin, Type synthesis of parallel mechanisms, Springer Publishing Company, Incorporated, 2007